Low power 3 degree-of-freedom Lorentz force MEMS mirror for optical applications

Elnaz Afsharipour,[a,*] Ramin Soltanzadeh,[a] Byoungyoul Park,[a] Dwayne Chrusch,[a] Cyrus Shafai[a]

[a]University of Manitoba, Faculty of Engineering, Dept. of Electrical and Computer Engineering, 66 Chancellors Circle, Winnipeg, Canada, R3T 5V6

Abstract. A low power three-degree-of-freedom scanning micro-mirror is presented. The 2×2 mm mirror is a gimbaless structure, directly supported by single crystal micro-springs. It is actuated by Lorentz force and is able to tilt about two axes and has linear motion in a third axis. The transient and frequency responses of the micro-mirror are analyzed. The Lagrange's equations of motions, describing the dynamic behavior of the system are presented, and show a good agreement with the experimental results. The fabricated MEMS mirror demonstrated a tilt angle of 22.8º at 247.5 Hz about *y*-axis, and 13.3º at 292.7 Hz about *x*-axis, in a 0.1 T magnetic field and 20 mA current on the mirror. Power consumption was 2.6 mW of power in tilting motions in resonant operation. With a total dc drive current of 110 mA, 232 μm linear motion was achieved.

Keywords: MEMS mirror, scanning micro-mirror, Lorentz actuator, electromagnetic actuator, 3- degree of freedom

Elnaz Afsharipour, Ramin Soltanzadeh, Byoungyoul Park, Dwayne Chrusch, Cyrus Shafai, "Low-power three-degree-of-freedom Lorentz force microelectromechanical system mirror for optical applications," J. Micro/Nanolith. MEMS MOEMS 18(1), 015001 (2019), doi: 10.1117/1.JMM.18.1.015001.

1 Introduction

Directing light beams is the working principle of many optical systems, including spectrometers[1], imaging systems[2, 3], micro-projectors[4], optical telecom[5, 6] and optical sensors[7]. Scanning micro-mirrors moved by Micro-electromechanical system (MEMS) actuators have been used for this purpose in many works. Depending on the application, a MEMS mirror is characterized by its degree of freedom (DOF) in motion, amplitude of movement, response time, scanning resolution, power consumption and size. Multi-DOF micro-mirrors are usually categorized in three types. The

first type has two tilting motions (2-DOF)[4,5,8,9], the second type has two tilting motions and one linear motion (3-DOF)[10,11,12], and the third type has two tilting motions and radius-of-curvature changing feature (3-DOF)[6,13,14,15]. The second and third types which have 3-DOF are usually enhanced versions of the first type. These types of micro-mirrors have mostly been used in medical imaging tools[16] such as endoscopic catheters for optical coherent tomography (OCT)[3, 8, 15], and Michelson interferometer of Fourier transform spectroscopy[17, 18]. In some of these applications, a large amplitude of motion is required. For example, in endoscopic catheters the micro-mirror is intended to scan its surrounding area, therefore a larger angle can be scanned which provides more data. In case of Michelson interferometer, it makes the splitting ratio more stable over a wider range of wavelengths[17]. Varifocal micro-mirrors can focus the light beam on a larger range of focal length which makes a high resolution possible at different depths[14]. Therefore, efforts towards improving the design of multi DOF micro-mirrors to achieve large amplitude of motion has attracted a lot of attention.

These large-tilt-angle multi-axis mirrors have been reported in many configurations of actuation forces and mechanical structures. They are designed either by cascaded-frames design which enables two perpendicular motions (gimbaled)[4, 9] or by using flexures connecting the mirror to a frame (gimbal-less)[10, 12]. In terms of actuation mechanism, all the four main actuation forces in MEMS including electrostatic[4], electromagnetic[9, 11, 19], thermal[10, 12], and piezoelectric[20] have been employed for moving the micro-mirrors.

Electrostatic actuators have been widely used for micro-mirrors due to their low power consumption and compact package. However, for a larger displacement they need a high input voltage. For example, Li et al.[21] used a lever-based structure working in resonance to amplify the

amplitude of motion. A translational displacement of > 400 μm was achieved with an applied voltage of 80 V.

Electro-thermal and electromagnetic actuators have proved to be very efficient in making large tilt angle and high DOF. Many attempts were done to solve the problem of high temperature on the flexures in the conventional electro-thermal devices. For example, Toress et al.[22] examined the vanadium dioxide as the flexures material. VO_2 undergoes a phase transition in a certain temperature that causes a change in its physical characteristics. Using VO_2, the temperature was reduced from 300°C to 90°C. This temperature range can be fine for devices which are not sensitive to heat or the ones with heat dissipate system. However, temperature-sensitive systems still need micro-mirrors that generate less heat than the suggested design.

Electromagnetic actuators have also been developed to achieve large and multidimensional motion. However, in most of these cases the micro-mirror has only 2 DOF, because of the physical limit caused by the orientation of the magnetic field and direction of the current. To our best knowledge, in electromagnetically actuated micro-mirrors, the largest reported optical tilt angle is 118° which belongs to Makishi et al.[23]. This angle was achieved by applying a current of 250 mA. This 2-DOF mirror consisted of 4 coils located at 4 sides of the mirror, for generating magnetic field. This design provided configurable and strong magnetic field, but enlarged the final footprint of the device and increased the power consumption. In another study, the micro-mirror developed by Yalcinkaya et al.[24] provided large tilt angles of 65° and 53°, which were achieved by applying a current of 150 mA in the dynamic mode. The micro-mirrors developed by Sung et al.[25] and Jeong et al.[26] were able to tilt up to 20° at 10 mW and 30° at 60 mW, respectively. However, they can generate a 2-dimensional pattern of light, in the dynamic mode and do not offer static control over the tilt angle. The micro-mirrors developed by Cho et al.[11] and Ataman et al.[27] offered a 2-

dimensional static control over the tilt angle of the mirror and could tilt up to 4.2°/ 9.2° and 16° respectively. However, these angles were achieved by consuming a large power of more than 300 mW and 5 W respectively.

In this work, we present a 3-DOF micro-mirror which meets a fair trade-off between degree of freedom, tilt angle, power consumption, and static and dynamic modes of operation. The micro-mirror is actuated by Lorentz force and can tilt about two axes and has one linear motion. Comparing to the other works, the presented micro-mirror offers a lower power consumption, while still providing a large tilt angle and displacement in 3 dimensions. In a preliminary study[28], the feasibility of this design was investigated by a 3D finite element method (FEM) simulation model. In this paper, the dynamic modeling, fabrication, and experimental test results are presented. In the following sections, the working principle of the mirror is described and the fabrication process is explained. The experimental setup is explained and the static and transient responses of the micro-mirror are discussed. The Lagrange's equations are solved and compared to the practical results to explore the dynamic motion of the system.

2 Design

The design consists of a rectangular mirror which its corners are connected to a frame by four single crystal silicon serpentine springs. It is worthwhile to mention that the four serpentine springs are mentioned as flexures through this paper. Fig. 1a shows the schematic of the structure, the places of the springs and the orientation of the magnetic field. The structure was fabricated from a 5 μm thick silicon membrane as substrate, 100 nm thick silicon dioxide as insulator and 1.6 μm aluminum top surface for the electrical conductor and mirror. The fabrication process is explained in detail in next section.

Fig.1b shows the electrical conduction wires passing on top of the flexures and mirror sides. The magnetic field was applied by an external permanent magnet. The generated Lorentz force is governed by (1).

$$\vec{f} = \vec{I}l \times \vec{B}, \tag{1}$$

where I is the current, l is the length of wire and B is the magnetic flux density. The direction of the magnetic field was perpendicular to flexures 1 and 3 and making a 45º angle with the mirror sides. This configuration of magnetic field direction and geometrical structure, shown in Fig.1, was designed to exert the maximum force on flexures 1 and 3, while there will be no force on flexures 2 and 4. Also, in this configuration, a uniform force is applied on all four mirror sides.

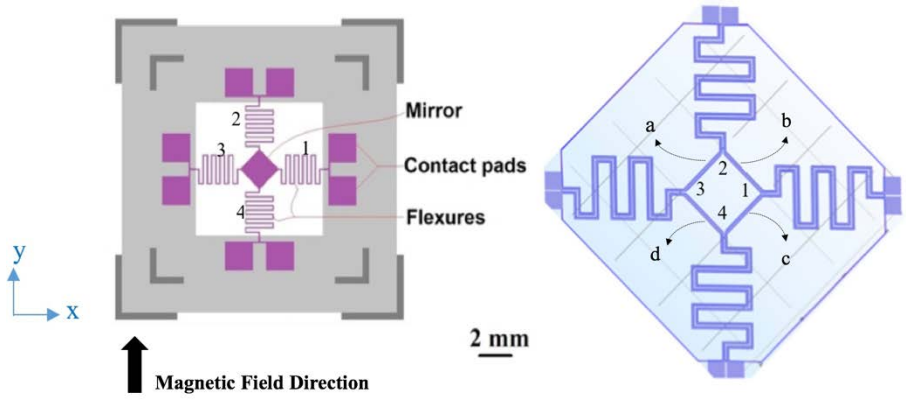

(a) (b)

Fig. 1 (a) Schematic of the MEMS mirror. (b) Path of aluminum wires.

The mirror can move in three degrees of freedom including tilting about *x*- axis, tilting about *y*- axis, and translational motion in z-axis. There are four wire paths shown in Fig. 1b, that pass through the mirror and springs. The direction of the Lorentz force applied on each side of the mirror, is changed by the direction of the current passing through each wire path. When the current passing through the sides *a* and *b* make an out-of-plane force, and the current passing through the

sides *c* and *d* make an in-plane force, a tilt motion about *x* axis is generated. In the same way, when the current passing through the sides *a* and *d* make an out-of-plane force and the current passing through the sides *b* and *c* make an in-plane force, a tilt motion about *y* axis is generated. If the current passing through all the four actuators makes the same direction of force, a translational motion in *z* axis generated.

3 Fabrication

The micro-mirror was fabricated using bulk and surface micromachining techniques. The process flow is shown in Fig. 2. A 4-inch, (100) silicon wafer with a thickness of 300 μm was used. A layer of 1.5 μm silicon dioxide was thermally grown on both sides of the wafer (step 2 of Fig. 2). Optical lithography was used to pattern the oxide on the backside of the wafer (step 3 of Fig. 2). The bulk silicon was etched using potassium hydroxide (KOH) solution to thin the wafer to a thickness of 25 μm (step 4 of Fig. 2). The old oxide layer was etched and a new layer of 100 nm insulator oxide was thermally grown on both sides of the wafer (step 5 of Fig. 2). A thin layer of titanium was deposited as adhesion layer using dc magnetron sputtering. A layer of 1.6 μm aluminum was deposited on the front side of the wafer using thermal evaporation (step 6 of Fig. 2). The residual stress of aluminum right after deposition was measured 42 MPa using a Toho FLX-2320 thin film stress measurement system. It was patterned to form the wires and mirror on the front side of the wafer (step 7 of Fig. 2). The patterned frontside was covered by a thick layer of photoresist, and anisotropic RIE plasma etching was done to etch the silicon from the frontside for 5 μm depth, corresponding to the final desired thickness of the structures (step 8 of Fig. 2). After this step, the thickness of the silicon mirror and springs under the photoresist protected area was 25 μm, and the thickness of silicon at all the other areas was 20 μm. By knowing the isotropic RIE etch-rate, the etch time for etching 20 μm of silicon was calculated. The wafer was flipped

over and the etch time was set to remove a thickness of 20 µm of silicon (step 9 of Fig. 2). The device was constantly watched to check the process of etching. After the thinned silicon was etched, the flexures were released from the backside. At the end, a layer of 5 µm silicon under the mirror and spring area was left (step 10 of Fig. 2). Fig. 3a shows microscopic image of a fabricated MEMS mirror. A closer view of a flexure is shown in Fig. 3b.

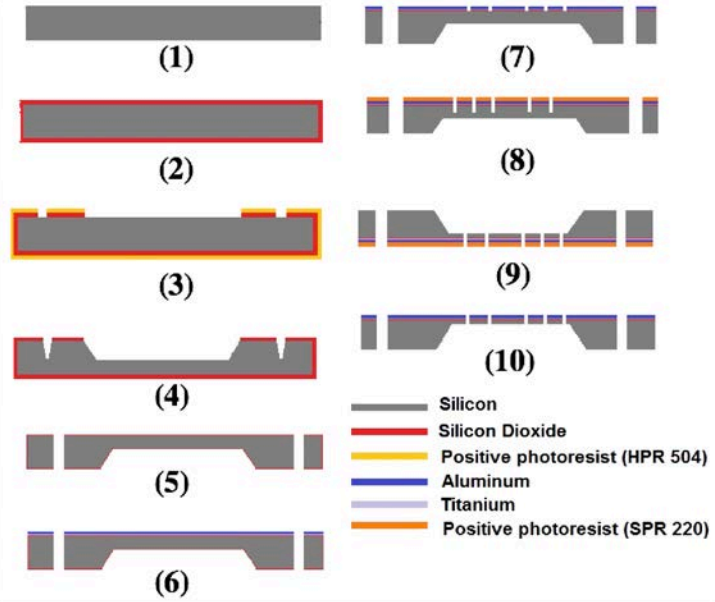

Fig. 2 The fabrication steps of the micro-mirror.

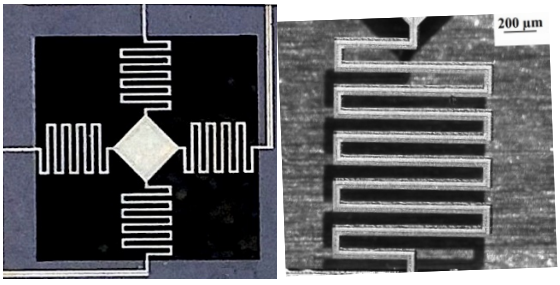

(a) (b)

Fig. 3 Pictures of the fabricated device, showing no easily visible stress deformations. (a) Picture of the fabricated MEMS mirror. (b) Closer view of a flexure.

3.1 Static deformation

The mirror shown in Fig. 3a was inspected under microscope to determine its flatness. The height difference between the four corners and the center of the mirror was measured. The maximum height difference was measured to be 32 μm. The average height difference on the mirror surface was 9 μm which is about 0.45% of the mirror length.

4 Experimental Procedure and Results

Fig. 4 a. shows the setup used for testing the device. A *PTI Technologies PM01 (635-5B) G3* laser diode was used to shine light on the mirror and an *API SD380-23-21-051* photodetector was used to detect the reflected light. The magnetic field generated by an N42 (BY08Y0, K&J Magnetics) permanent magnet was measured using a gaussmeter (model *G2*, AlphaLab INC.) at the location of the micro-mirror, which was placed over the center of the magnet. The electrical resistivity of the Al wires after contact pads and connector wires was measured 26.4 Ω, following route a of Fig 1b, which includes the mirror and two wire paths on the spring 2 and 3 of Fig 1a. All experiments were done in a closed box and on a vibration isolation table to minimize environmental optical and mechanical noise. The permanent magnet was fixed on the floor of the box. For these experiments the amplitude of the magnetic field at the location of mirror was measured to be 0.1 T. A compass was used to observe the orientation of the magnetic field. The side borders of the mirror frame was aligned to be parallel to the magnetic field direction using a ruler.

Fig.4b shows a schematic of the light beams when the mirror is tilted with a mechanical angle of θ_M. The light incident angle θ_i was set to be 45º with respect to the normal to the substrate plane. The angle of the reflected light beam is equal to $\theta_i + 2\theta_M$ with respect to the normal to the substrate

plane. The amount of deflection of the laser beam, is equal to the difference between the new reflection angle ($\theta_i + 2\theta_M$) and the previoues reflection angle (θ_i) which is $2\theta_M$. This value is known as optical deflection or tilt angle (θ) and used in this paper.

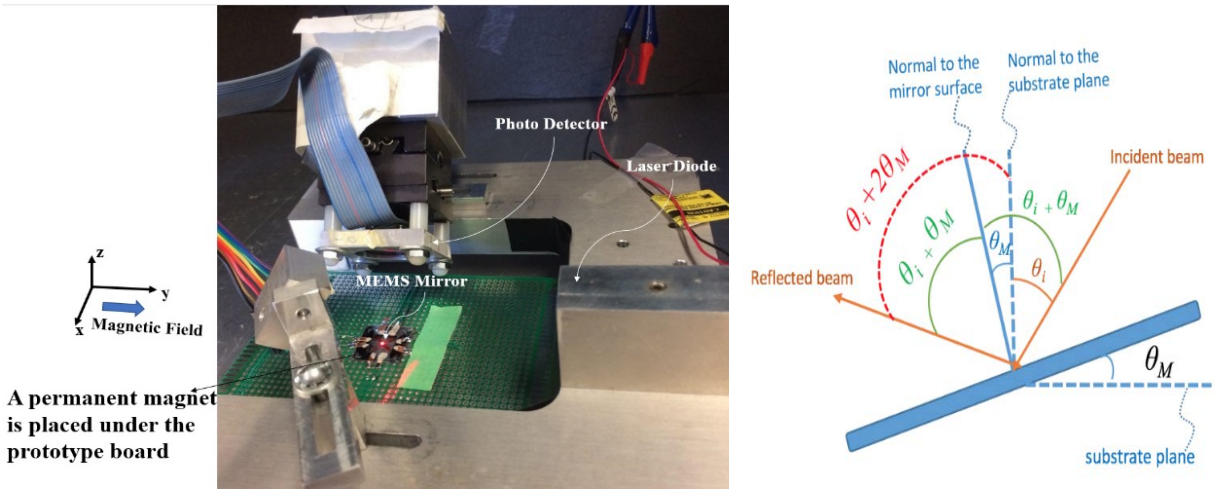

(a) (b)

Fig. 4 (a) Experimental setup used for characterizing the structure. (b) Schematic of the beams when the mirror is tilted.

4.1 Transient response

A current step-function rising from 0 to 137 mA was applied to device. To supply and adjust the dc current passing through the actuators, the setup of Fig. 5 was used. The setup included a computer interface, microcontroller system (Arduino UNO), two current driver ICs (SN7544) and ampere meter. The type of motion and the amount of current was set in the terminal environment of the computer and sent to the microcontroller through a serial port. According to the received data, a Pulse-Width-Modulation (PWM) signal was generated by the microcontroller system and sent to the current driver ICs. This IC includes two half-H drivers which can change the direction of the current and support a high current of up to 1A. Each IC supports two actuators. The amplitude of current was controlled by the duty cycle of the PWM pulse. Simulation showed that

the heat generated by a current of 20 mA passing through each of the four actuators, results in a temperature rise of 7.7º on the mirror. This causes a curvature of ~22 µm, which is equal to ~0.8% of the mirror diagonal. In all the experiments, the current was limited to keep the mirror bending displacement lower than 1% of the mirror diagonal. An ampere meter was placed in the branch of each actuator to ensure the right amount of current is passing through the actuators. By knowing the amount of current and resistivity of the wires, the consumed power was calculated.

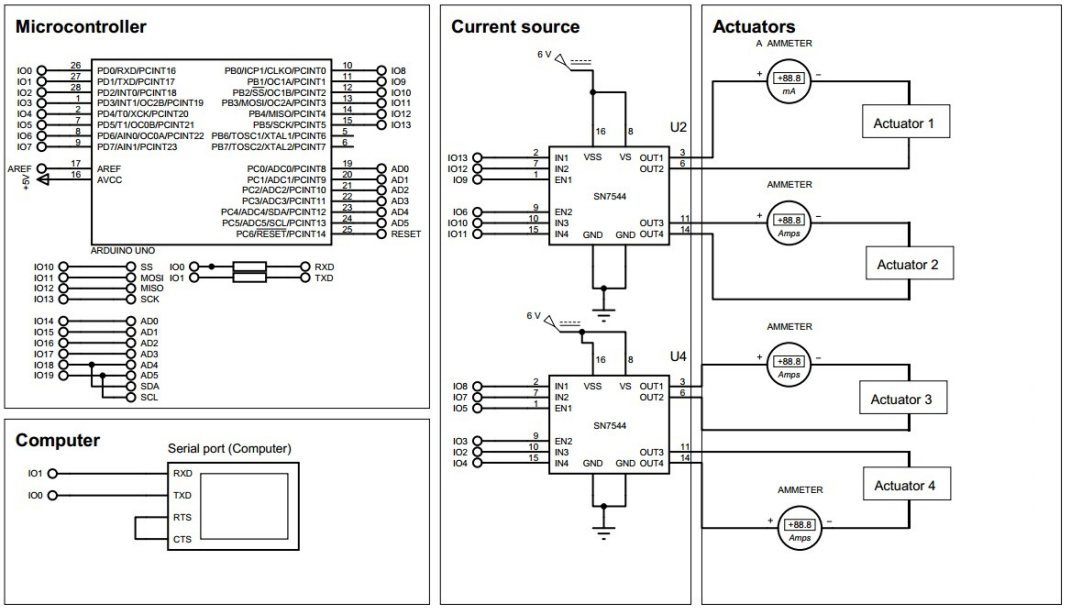

Fig. 5 Schematic of the setup used for generating dc current

The output of the photodetector was captured on oscilloscope. Fig. 6. shows the step response of the device while tilting about the *y*-axis, for the current step-function rising from 0 to 137 mA. This step response demonstrates a second order system. Therefore, we can model the system accordingly. The transfer function of the system can be written as:

$$G(S) = \frac{{\omega_n}^2}{S^2+2\xi\omega_n S+{\omega_n}^2} \tag{2}$$

where ω_n is the natural frequency and ξ is the damping ratio of the system. From the step response data of Fig. 6., we can see that the time between two peaks is 4 ms. Therefore, the natural frequency is found to be:

$$\frac{2\pi}{\omega_n} = 4\ ms \rightarrow\ \omega_n = 1551.8\frac{rad}{s}\ or\ 247\ Hz \tag{3}$$

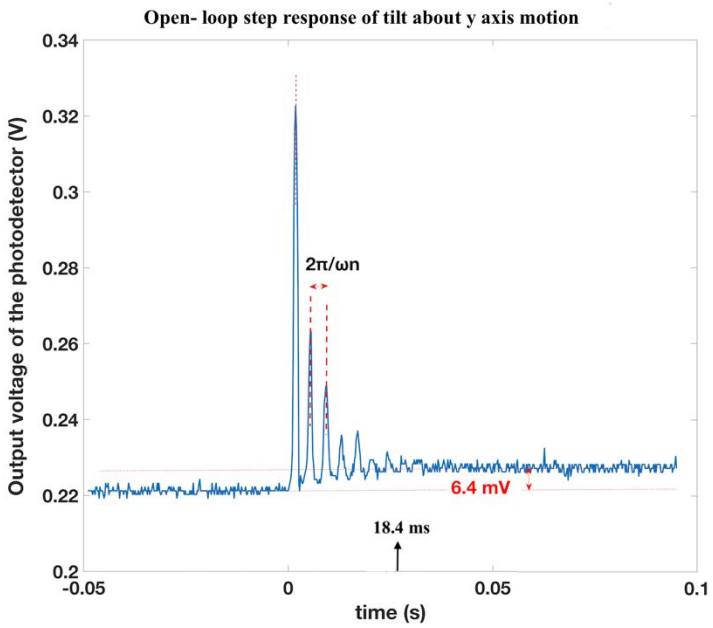

Fig. 6 Open-loop step response of the tilt about *y*-axis motion.

From the graph of Fig.6 peak time was read to be 2 ms. The peak time was used to calculate the damping ratio or ξ of the system.

$$t_p = \frac{\pi}{\omega_n\sqrt{1-\xi^2}} \rightarrow\ \xi = 0.14 \tag{4}$$

Settling time was calculated using (5):

$$t_s = \frac{4}{\xi_2\omega_n} = 18.4\ ms \tag{5}$$

Therefore, for ξ = 0.14 and ω_n =1551.8 rad/s, the transfer function of the system was written as below:

$$G(S) = \frac{(1551.8)^2}{S^2+434.5\,S+(1551.8)^2} \tag{6}$$

4.2 Operation in a driven axial direction

Various angles of tilting of the mirror were measured by applying a dc current of different amplitudes, and observing the motion of a reflected laser spot. Fig. 7 plots the tilt angle vs. applied current for *x*-axis and *y*-axis tilting motions. The larger tilt angle of the tilt-about-*y*-axis motion can be explained by the focre applied on the springs number 1 and 3. According to Fig. 1a the magnetic field orientation is parallel to the *y* axis and perpendicular to the *x* axis. According to Equation (1), there is a large force on springs number 1 and 3 of Fig. 1a, since they are perpendicular to the magnetic field. While there is no force on springs 2 and 4, since they are parallel to the magnetic field. When the mirror is tilting about the *y* axis the force on springs 1 and 3 along with the force on all the four sides of the mirror, contribute in the motion. However, when the mirror is moving about *x* axis, there is no force on springs 2 and 4, so the only force moving the miror is the force applid on the mirror sides. Therefore, in tilt-about-*x* axis motion the force is less than the tilt-about-*y*-axis motion which resuts in a lower ampliude of displacment.

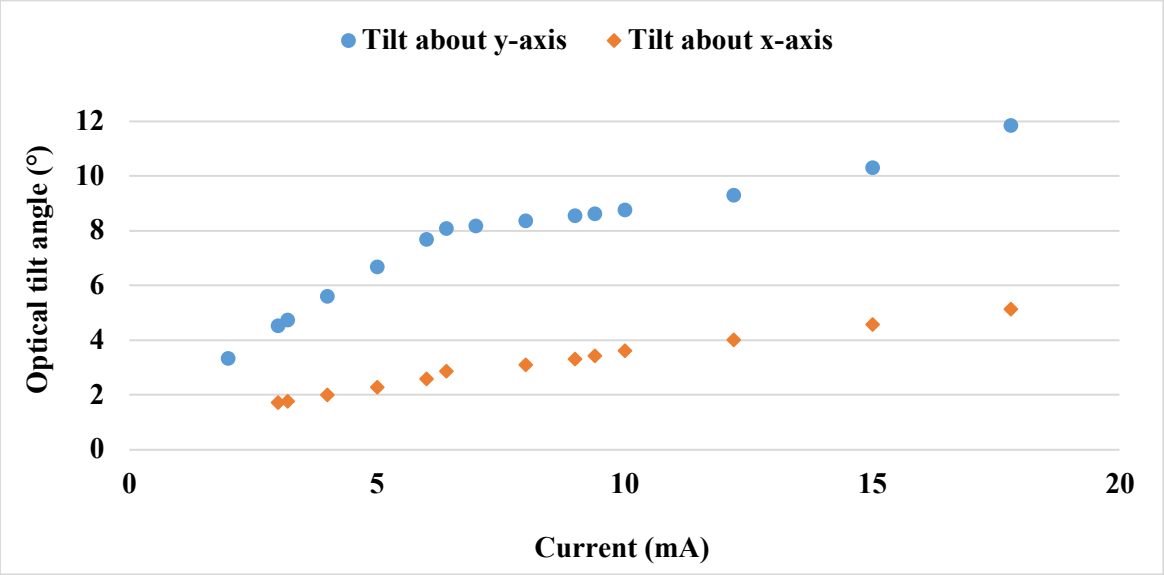

Fig. 7 Optical tilt angle vs applied current of the *y*-axis and x-axis tilting motions.

Translational motion in *z* axis was measured by observing the mirror under an optical microscope. First, the objective lens was focused on one point of the mirror. Then, a current was applied and the mirror was actuated in *z* direction. While the mirror was in the actuated mode, the objective lens was focused again, on the same spot. The distance between the first and second focal points was measured by measuring the displacement of the microscope stage in *z* axis. This distance was recorded as the *z* axis displacement of the mirror. Fig. 8 shows the graph of translational motion in. *z* axis versus applied dc current to each actuator. The horizontal axis shows the amount of current passing through each actuator. The translational motion along the *z*-axis was measured to be 232 µm with a total applied current of 110 mA (27.5 mA each actuator), which equals to 20 mW of power per actuator. Considering the range of motion with respect to the consumed power, this motion is larger than what has been reported in the literature for 3D micro-mirrors (as will be discussed in section 5).

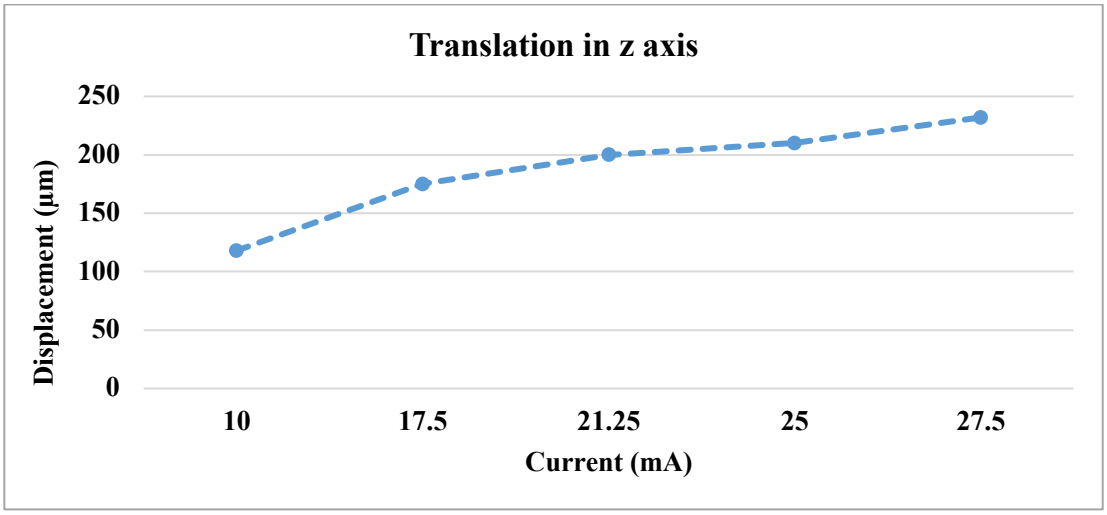

Fig. 8 Translation motion along *z* axis vs applied current, with this current applied to each of the four actuators.

4.3 Frequency response

The resonance frequency of the mirror in *y*-axis and *x*-axis tiltings were practically measured by applying a 50 mV_{p-p} sinusoidal wave to appropriate terminals of varying frequency between 1 to 500 Hz. A lock-in amplifier (Stanford Research System SR830) was used to filter the noise of other frequencies. The output of the photodiode was measured using a digital multimeter (34461A Keysight Technologies). A block diagram of the measurement setup is shown in Fig. 9.

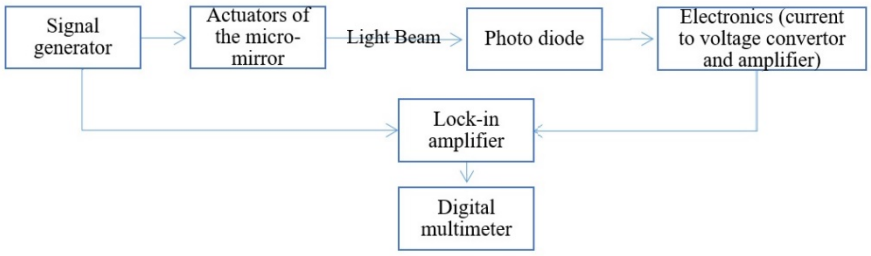

Fig. 9 Block diagram of the experimentral setup for measuring the resonance frequency.

The resonance frequency of the *y*-axis and *x*-axis tilting motions were measured in two separate experiments. The blue line on the graph of Fig. 10 shows the measured frequency response of the *y*-axis tilting motion. The maximum displacement occurred at 247.5 Hz which is the resonance frequency of the structure while the mirror is tilting about *y*-axis. The red dashed line shows the simulated FEM frequency response of the structure. The measured displacement for tilting about *x*-axis (292.7 Hz resonance) and *y*-axis (247.5 Hz resonance) are summarized in Table 1. The *z*-axis translation resonance was observed to be 165 Hz.

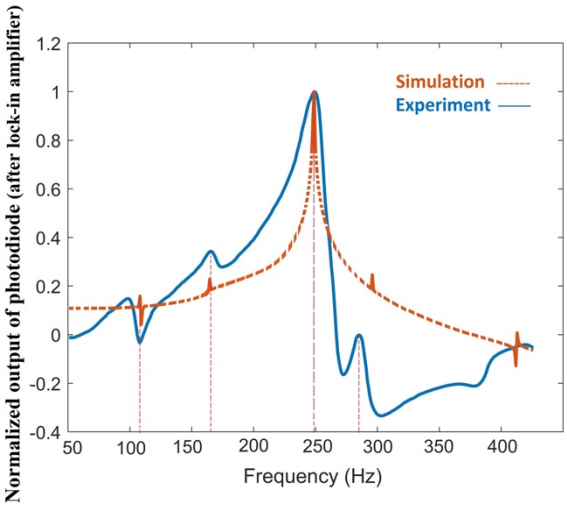

Fig. 10 Frequency response of the tilt about *y*-axis motion, and resonance frequency was at 247.5 Hz.

At the resonance frequencies shown in Table 1, the light pattern on the screen was a horizontal line for the *x*-axis tilting, and a vertical line for the *y*-axis tilting. Fig. 11 shows the pattern of reflected light at the main resonance frequencies of the horizontal (tilt about *x*) and vertical (tilt about *y*) scanning motions.

Table 1 Mechanical tilt angle and displacement of *y*-axis and *x*-axis tilt motions in a magnetic field of 0.1 T.

Motion type	**Freq.**	**Power consumption / current (rms)**	**Amplitude of motion**
Tilt about *y-axis (Vertical)*	247.5 Hz	2.6 mW/ 20 mA	22.8º
Tilt about *x-axis (Horizontal)*	292.7 Hz	2.6 mW/ 20 mA	13.3º

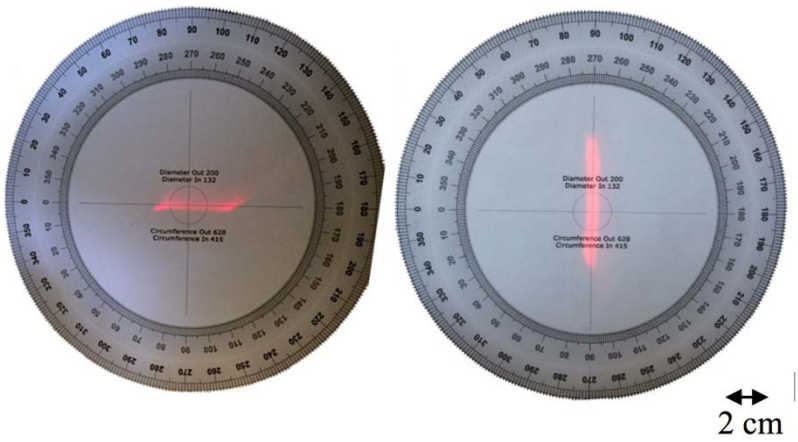

(a) (b)

Fig. 11 (a) Horizontal scanning (tilt about x-axis). (b) Vertical scanning (tilt about *y*-axis).

4.3.1 Dynamic deformation:

Dynamic deformation of a scanning mirror occurs when a mirror is tilting with a high frequency. The high acceleration caused by alternating forces on the mirror surface might result in mechanical bending on the mirror. The maximum dynamic deformation was calculated using (7) for a rectangular shaped mirror [29, 30, 31]:

$$\delta = \frac{0.288\,\rho\theta_0\omega^2 L^5}{Et^2} \tag{7}$$

where δ is the dynamic deformation, ρ is the material density, θ_0 is the mechanical tilt angle of the mirror, ω is the tilting frequency, L is the half-length of the mirror, t is the thickness of mirror and E is the young's modulus of the mirror material. The dynamic deformation is calculated using the experimentally found values for the mirror tilting about *y*-axis (resonance frequency 247.5 Hz, mechanical angle of 11.4º), and is found to be 1.4 µm. This value is 0.07% of the mirror length.

To see if the value calculated for the dynamic deformation, is reasonable, we can consider how the resonance of mirror and spring elements compare. The simulated values from COMSOL show the resonance frequency of the mirror to be 2258 Hz, and the resonance frequency of the spring to

be 214.5 Hz. Experimentally, the total system resonance frequency was measured to be 247.5 Hz for the *y*-axis-tilt motion, which is close to spring resonance frequency. Therefore, it is reasonable to assume that there is low dynamic deformation of mirror, since the mirror resonance is more than 9× higher than the measured system's resonance.

4.3.2 Raster Scanning:

By actuating one axis in resonance mode and the other axis in a lower frequency, a raster scan pattern can be generated. Fig. 12 shows a raster scan which was made by enabling horizontal scanning (*x*-axis tilting) at its resonance frequency 292.7 Hz and vertical scanning (*y*-axis tilting) at 40 Hz.

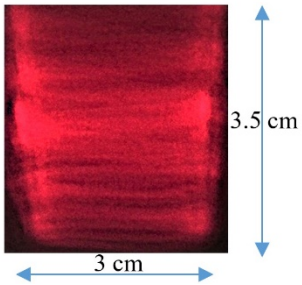

Fig. 12 Raster scan pattern, the horizontal axis resonating at its resonance frequency 292.7 Hz and the vertical axis tilting at 40 Hz.

4.3.3 Mode Coupling:

However, at some specific frequencies a multi-axial motion can be seen. This indicates that some coupling is occurring between the different axial motions. In order to understand how this can occur, a modal analysis was done using Lagrange's equations. Lagrange's equations of motion (8) were used to formulate the differential equations that describe the dynamic response of the system[32],

$$\frac{d}{dt}\left(\frac{\partial L}{\partial \dot{q}_i}\right) - \frac{\partial L}{\partial q_i} = 0 \tag{8}$$

where L= K - P, and *K* is the kinetic energy, *P* is the potential energy, q_i are coordinates of the four corners shown in Fig. 1.b, and q_i dotted are velocities of the four corners. The kinetic energy includes three motions of the mirror, two tilting motions and one translational given by,

$$T = \frac{1}{2}m(\dot{u}_z)^2 + \frac{1}{2}J_x(\dot{\theta}_x)^2 + \frac{1}{2}J_y(\dot{\theta}_y)^2 \tag{9}$$

where u_z is the displacement of the center of the mirror in z-axis, θ_x and θ_y are tilt angles about x and y axes. J_x, J_y and m are the moments of inertia and mass of the suspending structure. The potential energy consists of the energy stored in the four springs while bending or torsion. The potential energy of the four points on the corners of the mirror due to bending are given by:

$$\begin{aligned} U_{bending} = {} & \frac{1}{2}k_{f_z-u_z}{u_{1z}}^2 + \frac{1}{2}k_{M_y-\theta_y}{\theta_y}^2 + k_{f_z-\theta_y}u_{1z}\theta_y \\ & + \frac{1}{2}k_{f_z-u_z}{u_{2z}}^2 + \frac{1}{2}k_{M_x-\theta_x}{\theta_x}^2 + k_{f_z-\theta_x}u_{2z}\theta_x \\ & + \frac{1}{2}k_{f_z-u_z}{u_{3z}}^2 + \frac{1}{2}k_{M_y-\theta_y}{\theta_y}^2 + k_{f_z-\theta_y}u_{3z}\theta_y \\ & + \frac{1}{2}k_{f_z-u_z}{u_{4z}}^2 + \frac{1}{2}k_{M_x-\theta_x}{\theta_x}^2 + k_{f_z-\theta_x}u_{4z}\theta_x \end{aligned} \tag{10}$$

The potential energy due to torsion is:

$$U_{tor} = \frac{1}{2}k_{T_x-\theta_x}{\theta_x}^2 + \frac{1}{2}k_{T_x-\theta_x}{\theta_x}^2 + \frac{1}{2}k_{T_y-\theta_y}{\theta_y}^2 + \frac{1}{2}k_{T_y-\theta_y}{\theta_y}^2 \tag{11}$$

where u_{iz} is the z-axis displacement of the corner number i shown in Fig. 1.b, and $k_{M_x-\theta_x}$ means the resistance of the spring to tilting about the x-axis when a moment of bending about the x-axis is applied to it. In the same way, $k_{f_z-\theta_y}$ means the resistance of spring to tilting about the y-axis when a force in the z-axis is applied to it, and $k_{T_x-\theta_x}$ is the torsional spring constant. This labeling is applied to all the k parameters. All the values of k and $J_{x\ and\ y}$ were obtained using a finite element simulation in COMSOL software by applying a force or torque on the mirror and springs, and measuring the corresponding displacement or tilt angle. The values are presented in Table 2.

Table 2 Spring constants and moment of inertia values of the structure.

$k_{f_z-u_z}$	0.06 N/m

$k_{M_y-\theta_y}$, $k_{M_x-\theta_x}$	$1.9\times10^{-4} \pm 2\%$ N·m/rad
$k_{f_z-\theta_x}$, $k_{f_z-\theta_y}$	$8.2\times10^{-5} \pm 2\%$ N/rad
$k_{T_x-\theta_x}$, $k_{T_y-\theta_y}$	$2.6\times10^{-8} \pm 2\%$ N·m/rad
J_x, J_y	1.4×10^{-10} kg·m^2
m	2×10^{-7} kg

By substituting the kinetic and potential energy of equations (9), (10) and (11) in (8), writing the displacement of each corner (u_{iz}) as a function of displacement of the center (u_z) and taking derivations, the matrix form of Lagrange's equation was written as:

$$\begin{bmatrix} J_x & 0 & 0 \\ 0 & J_y & 0 \\ 0 & 0 & m \end{bmatrix} \begin{bmatrix} \ddot{\theta_x} \\ \ddot{\theta_y} \\ \ddot{u_z} \end{bmatrix} + \begin{bmatrix} 2R^2 k_{f_z-u_z} + 2k_{M_x-\theta_x} + 2k_{T_x-\theta_x} & 0 & 2k_{f_z-\theta_x} \\ 0 & 2R^2 K_{f_z-u_z} + 2k_{M_y-\theta_y} + 2k_{T_y-\theta_y} & 2k_{f_z-\theta_y} \\ 2k_{F_z-\theta_x} & 2k_{F_z-\theta_y} & 4k_{F_z-u_z} \end{bmatrix} \begin{bmatrix} \theta_x \\ \theta_y \\ u_z \end{bmatrix} = 0 \tag{12}$$

where R is the distance between the corners and the center. Therefore, the dynamic equations of motion can be written as:

$$\frac{d^2\theta_x}{dt^2} = -\left(\frac{2R^2 k_{f_z-u_z} + 2k_{M_x-\theta_x} + 2k_{T_x-\theta_x}}{J_x}\theta_x(t) + \frac{2K_{f_z-\theta_x}}{J_x}u_z(t)\right) \tag{13}$$

$$\frac{d^2\theta_y}{dt^2} = -\left(\frac{2R^2 K_{f_z-u_z} + 2k_{M_y-\theta_y} + 2k_{T_y-\theta_y}}{J_y}\theta_y(t) + \frac{2K_{f_z-\theta_y}}{J_y}u_z(t)\right) \tag{14}$$

$$\frac{d^2u_z}{dt^2} = -\left(\frac{2k_{F_z-\theta_x}}{m}\theta_x(t) + \frac{2k_{F_z-\theta_y}}{m}\theta_y(t) + \frac{4k_{F_z-u_z}}{m}u_z(t)\right) \tag{15}$$

These differential equations were solved using MATLAB. The resonance frequencies ω of the system were found to be 244.4 Hz for *y*-axis rotation, 287.6 Hz for x-axis rotation, and 174.3 Hz for z-axis translation, by solving eigenvalues of $[M]^{-1}[k]$ matrix. The resonances of the *y*-axis and *x*-axis motion calculated from these equations, are very close to the experimentally found resonances shown in Table 1.

The equations (13-15) show that the motions in the three axial directions are coupled, meaning that motion in any one axis gives a contribution to the other axial motions. This contribution is not significant unless the input frequency is close to the resonance frequency of one of the other axial motions. In the case when the motion approaches the resonance frequency of another axial direction, the motion in the other axial direction becomes significant, and so the overall movement of the mirror would include more than one axial direction. For example, to illustrate the effect of resonance frequency of *y*-axis on the resonant motion of the *x*-axis tilting, the *x*-axis was actuated with the resonance frequency of the *y*-axis. Fig. 13.a shows the light pattern when the mirror is resonating about *x*-axis at 292.7 Hz (its resonance). In Fig. 13.b the FEM simulation of the device displacement shape when tilting about *x* axis at the resonance frequency of 292.7 Hz can be seen. The frequency was changed to 247.5 Hz (y-axis resonance) while still in the *x*-axis tilting motion, the light pattern was approximately 40° tilted shown in Fig. 13.c. This is expected, as now motion from both axes would be significantly present. Fig. 13. d shows the FEM simulation of the device displacement shape when tilting about *x* axis at the frequency of 247.5 Hz. The motion of Fig.13.d consists of both components of tilting about *x* axis and *y* axis, although the mirror was actuated about *x* axis.

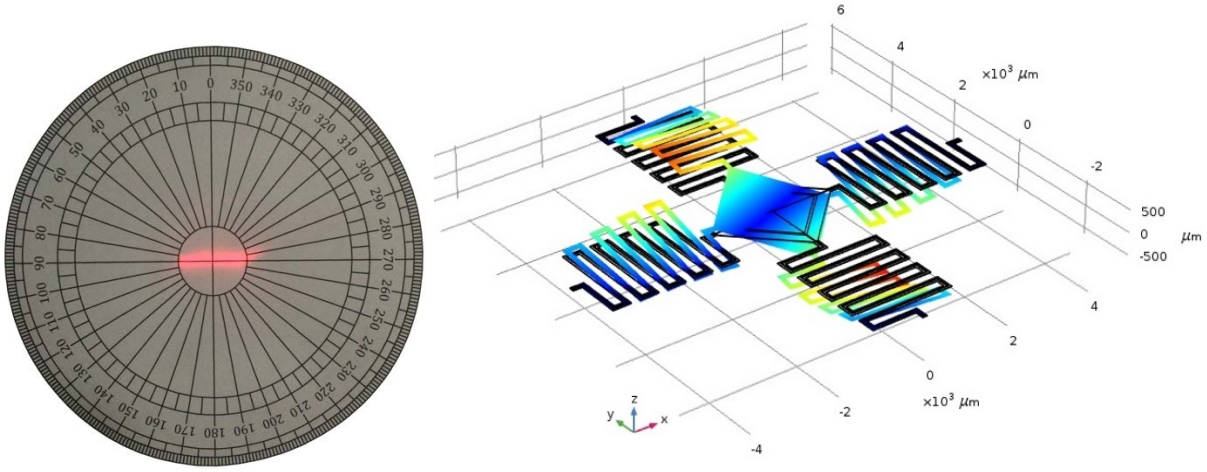

(a) (b)

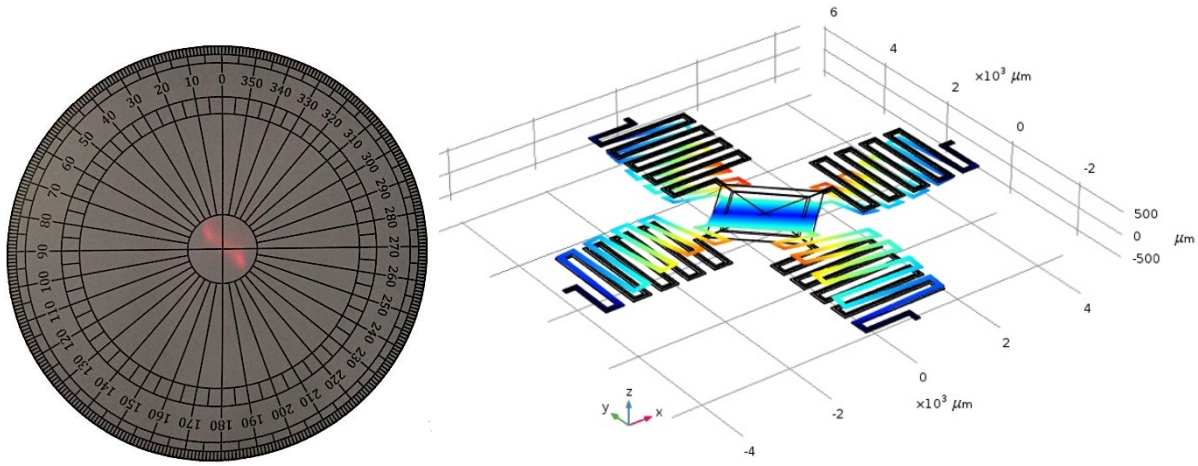

(c) (d)

Fig. 13 (a) Pattern caused by driving θ_x at its resonance of 292.7 Hz. (b) FEM simulation of mirror tilting about x axis at its resonance frequency of 292.7 Hz. (c) Pattern caused by driving θ_x at θ_y*'s* resonance of 247.5 Hz. (d) FEM simulation of mirror tilting about x axis at θ_y*'s* resonance of 247.5 Hz. The overal displacement is a combination of θ_x and θ_y motions.

To understand the patterns generated by the deflection shapes of the resonating mirror at the frequency modes which were discussed above, $\theta_x(t)$, $\theta_y(t)$, and $u_z(t)$ can be solved when an excitation is applied to any one axis. Fig. 14 plots the situation for an impulse applied to the system in the θ_y direction at time zero (system was prior stable), which then creates excitations at all frequencies. After finding $\theta_x(t)$ and $\theta_y(t)$ functions, θ_y versus θ_x was plotted on Fig. 14 by sweeping the time with intervals of 0.1s for 180 seconds. The various traces on the figure represent the dominant displacement of the mirror for each time step. The plot shows two main modes of vertical (y-axis tilt, green dashed line) and horizontal (x-axis tilt, red dashed line) overall motions, as well as an elliptical mode (z-axis translation, purple dashed line). These three dashed lines correspond to the main resonance modes of the mirror; green dashed line corresponds to 244.4 Hz (y-axis), red dashed line corresponds to 287.6 Hz (x-axis), purple dashed line corresponds to 174.3 Hz (z-axis). These modes were practically shown in Fig. 11 for y-axis and x-axis rotations.

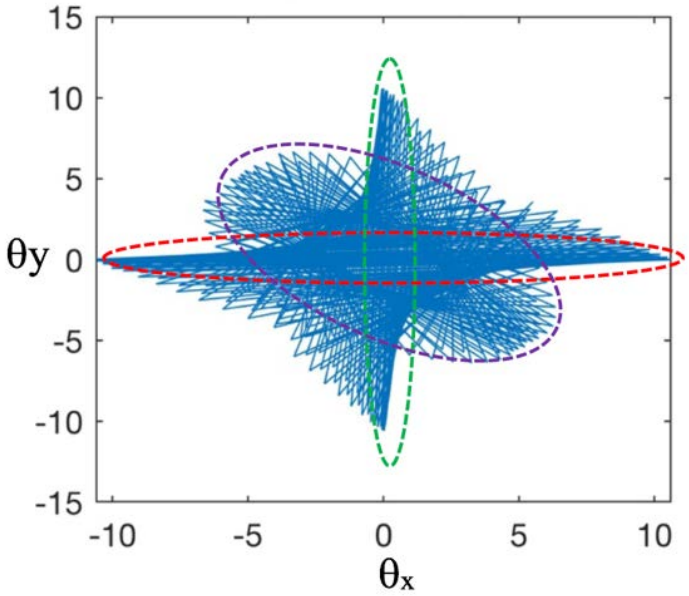

Fig. 14 Mode shapes derived by solving Lagrange's equations.

Following the above discussions, in Fig. 14 there exists a harmonic of elliptical shape (purple dashed line) that corresponds to the interference of *z*-axis translation. This resonance mode was experimentally observed at 165 Hz when driving θ_y at this frequency, as shown in Fig. 15.

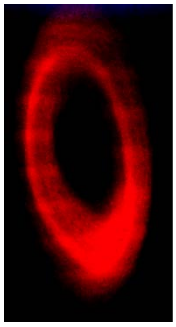

Fig. 15 Pattern caused by driving θ_y at 165 Hz.

From the modal analysis of this section, the light pattern at resonance modes of *y*-axis and *x*-axis motions were explained and compared with the practical results. The effect of mode coupling between different types of motion which results in an elliptical pattern of motion was also discussed. It could be concluded that if the mirror is supposed to scan horizontally or vertically, θ_x

or θ_y should be actuated at their resonance frequencies respectively. At these frequencies the vertical or horizontal motions are dominant. If an elliptical pattern is required, θ_y or θ_x can be actuated at the resonance of the *z*-axis.

5 Discussion

The design presented in this work features three main properties. First, a large tilt angle with respect to the input power is demonstrated. Second, three degree of freedom in motion is shown, which includes two tilting motions and one linear displacement. Third, this mirror design has the ability to work in both static (by applying a dc current) and in dynamic modes (by applying ac current with different frequencies). The main factors enabling 3-DOF large-tilt-angle motion are the geometrical design and actuation force of the actuator, enabled by the 4 serpentine flexures along with the 45º angle of the magnetic field with respect to the mirror sides. A tilt angle of 22.8° about *y*-axis, 13.3° about *x*-axis were achieved while consuming 2.6 mW of root-mean-square (rms) power in 0.1 T of magnetic field. A linear vertical displacement of 232 μm was also achieved by applying 110 mA of direct current (dc).

Table 3 summarizes some electromagnetically actuated large-tilt-angle MEMS-mirrors published by other groups, and the work presented in this paper. The paper by Cho et al.[11] also provides 3-DOF motion, but however, requires greater power consumption. For example, a translational motion of ±42 μm was achieved by consuming 345-360 mW. The micro mirror presented in this paper offers a translational motion of 232 μm with consuming 86.9 mW of power. The figure of merit defined as the ratio of optical tilt angle to the consumed power is calculated in Table 3, which shows high performance of this micro-mirror. The other listed works do not provide 3-DOF motion[33, 34]. The graph of Fig. 16 compares the performance of micro-mirrors reported in Table 3. The axes are plotted in logarithmic scale. The values of power consumption and mirror

size were inverted to show the lower power consumption and smaller mirror size farther from the center.

Table 3 Comparing characteristics of the electromagnetically actuated MEMS mirrors in the literature.

Ref. No.	Mirror size	Actuation force	DOF static / dynamic	Optical tilt angle / displacement	Power / current	FOM: $\frac{Opt.\ tilt\ angle(°)}{power\ (mW)}$
This work	2 mm × 2 mm	EM (MC) B = 0.1 T	3 S-D	22.8°, 13.3° at resonance z = 232 µm	2.6 mW / 20 mA 86.9 mW / 110 mA	8.7
[11]	900 µm × 900 µm	EM (MC) B = 0.16 T	3 S-D	±4.2°, ±9.2° z = ±42 µm	345-360 mW	0.03
[23]	8 mm × 4 mm	EM (MM)	2 S-D	118°	250 mA	0.47
[24]	1.5 mm	EM (MC)	2 D	65°, 53° at resonance	150 mA	0.43
[25]	~ 1 mm	EM (MM & MC)	2 D	20° at resonance	10 mW	2
[26]	3 mm × 1.5 mm	EM (MC)	2 D	30° at resonance	60 mW	0.5
[27]	4 mm × 4 mm	EM (MM)	2 S-D	±16°	5.12 W	0.003
[33]	1 mm × 1 mm	EM (MC)	1 S-D	25° at resonance	10 mW	2.5
[34]	1.5 mm	EM (MC)	2 S-D	8.8°, 8.3° at resonance	16.7 - 26.3 mW	0.41

EM: Electromagnetic, **MC**: Moving coil, **MM**: Moving magnet, **DOF**: Degree of freedom, **S**: Static, **D**: Dynamic, frequency, **B**= Magnetic Field

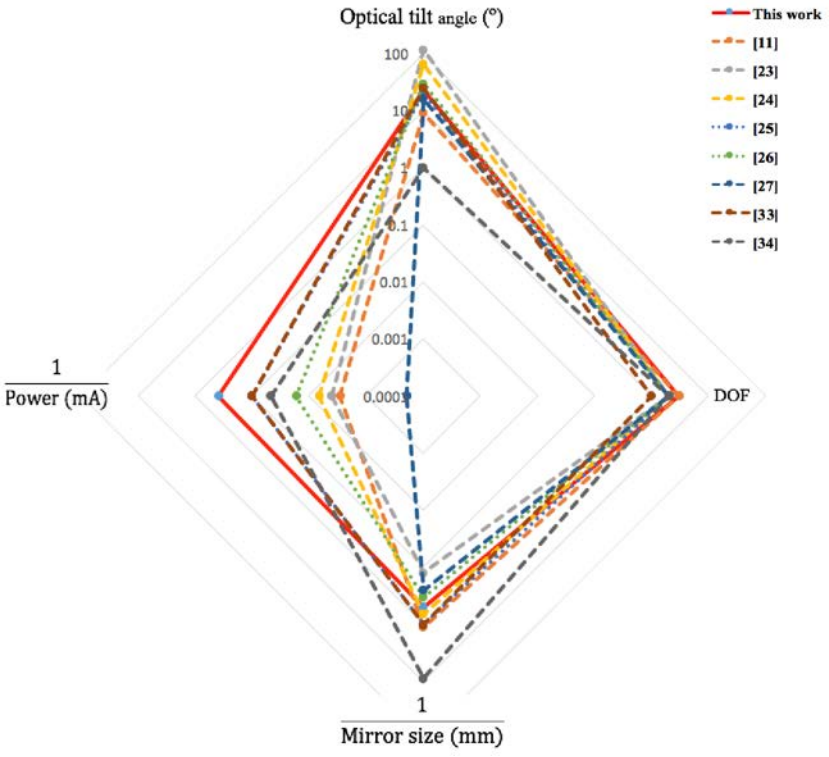

Fig. 16 Radar plot of the micro-mirrors reported in Table 3.

6 Conclusion

A MEMS mirror was developed which has three degree-of-freedom in motion. Lorentz force is used to actuate the structure. The micro-mirror is able to work in both static and dynamic modes. In static mode, a light beam is directed to one point by applying dc current to its flexures, while in the dynamic mode the mirror scans an area by resonating at its resonance frequency or one of its harmonics. With a magnetic field of 0.1 T, the MEMS mirror showed a tilt angle of 22.8º at 247.5 Hz, 13.3º at 292.7 Hz, while consuming 2.6 mW of power in tilt motions. A linear vertical displacement of 232 μm was achieved at 110 mA of dc current.

Disclosures

Authors have no financial interests in the manuscript and no other potential conflicts of interest to disclose.

Acknowledgments

This research was financially supported by the Natural Sciences and Engineering Research Council (NSERC) of Canada and the University of Manitoba Graduate Fellowship (UMGF).

References

1. Jianjun Chen, Yong Zhu, Wei Wei, Yang Li, Yining Yang, Ning Wang, and Jie Zhang. "Experimental Study of a Fourier Transform Spectrometer Based on Scanning Micro-Electromechanical Mirrors," *Spectroscopy Letters,* **48**(2), 96-100 (2015) [doi: 10.1080/00387010.2013.856327].
2. Reza Arablouei, Ethan Goan, Stephen Gensemer, Branislav Kusy, "Fast and robust pushbroom hyperspectral imaging via DMD-based scanning", Proc. SPIE **9948**, *Novel Optical Systems Design and Optimization XIX*, 99480A (27 September 2016) [doi: 10.1117/12.2239107].

3. Yingshun Xu, Janak Singh, Teo Hui Siang Jason, Kotlanka Ramakrishna, C. S. Premchandran, Chen Wei Sheng Kelvin, Chuah Tong Kuan, Nanguang Chen, Malini C. Olivo, and Colin JR Sheppard. "MEMS based non-rotatory circumferential scanning optical probe for endoscopic optical coherence tomography." In *European Conference on Biomedical Optics*, p. 6627_33. Optical Society of America (2007) [doi: 10.1364/ECBO.2007.6627_33].
4. Andrew C-L. Hung, Harrison Y-H. Lai, Ta-Wei Lin, Sheng-Gang Fu, and Michael S-C. Lu. "An electrostatically driven 2D micro-scanning mirror with capacitive sensing for projection display." *Sensors and Actuators A: Physical* **222**, 122-129 (2015) [doi: 10.1016/j.sna.2014.10.008].
5. V.A. Aksyuk, Pardo, F., Carr, D., Greywall, D., Chan, H.B., Simon, M.E., Gasparyan, A., Shea, H., Lifton, V., Bolle, C. and Arney, S. "Beam-steering micromirrors for large optical cross-connects." *Journal of lightwave technology,* **21**(3), 634 (2003) [doi: 10.1109/JLT.2003.811792].
6. Corey Pollock, Jessica Morrison, Matthias Imboden, Thomas DC Little, and D. J. Bishop. "Beam shaping with tip-tilt varifocal mirror for indoor optical wireless communication." *Optics Express,* **25**(17), 20274-20285 (2017) [doi: 10.1364/OE.25.020274].
7. Byoungyoul Park, Meiting Li, Sampath Liyanage, and Cyrus Shafai. "Lorentz force based resonant MEMS magnetic-field sensor with optical readout." *Sensors and Actuators A: Physical,* **241**, 12-18 (2016) [doi: 10.1016/j.sna.2016.01.032].
8. Sehui Kim, Changho Lee, Jin Young Kim, Geunbae Lim, Jeehyun Kim, Chulhong Kim, "A 2-axis Polydimethylsiloxane (PDMS) based electromagnetic MEMS scanning mirror for optical coherence tomography", Proc. SPIE 9698, *Advanced Biomedical and Clinical Diagnostic and Surgical Guidance Systems XIV*, 969812 (7 March 2016) [doi: 10.1117/12.2211928].
9. Ah Ran Cho, Aleum Han, Suna Ju, Haesoo Jeong, Jae-Hyoung Park, Inhoi Kim, Jong-Uk Bu, and Chang-Hyeon Ji. "Electromagnetic biaxial microscanner with mechanical amplification at resonance." *Optics express,* **23**(13), 16792-16802 (2015) [doi: 10.1364/OE.23.016792].

10. Jessica Morrison, Matthias Imboden, Thomas DC Little, and D. J. Bishop. "Electrothermally actuated tip-tilt-piston micromirror with integrated varifocal capability." *Optics express,* **23**(7), 9555-9566 (2015) [doi: 10.1364/OE.23.009555].
11. Il-Joo Cho, and Euisik Yoon. "A low-voltage three-axis electromagnetically actuated micromirror for fine alignment among optical devices." *Journal of Micromechanics and Microengineering,* **19**(8), 085007, (2009) [doi: 10.1088/0960-1317/19/8/085007].
12. Miguel Lara-Castro, Adrian Herrera-Amaya, Marco A. Escarola-Rosas, Moisés Vázquez-Toledo, Francisco López-Huerta, Luz A. Aguilera-Cortés, and Agustín L. Herrera-May. "Design and Modeling of Polysilicon Electrothermal Actuators for a MEMS Mirror with Low Power Consumption." *Micromachines,* **8**(7), 203 (2017) [doi:10.3390/mi8070203].
13. Yuhe Shao, David L. Dickensheets, Phillip Himmer. "3-D MOEMS mirror for laser beam pointing and focus control." *IEEE Journal of Selected Topics in Quantum Electronics,* **10** (3), 528-535 (2004) [doi: 10.1109/JSTQE.2004.828484].
14. R. Hokari, and K. Hane. "Micro-mirror laser scanner combined with a varifocal mirror." Microsystem technologies, **18(**4), 475-480 (2012) [doi: 10.1007/s00542-011-1416-6].
15. Matthew Strathman, Yunbo Liu, Xingde Li, and Lih Y. Lin.," Dynamic focus-tracking MEMS scanning micromirror with low actuation voltages for endoscopic imaging." *Optics express,***21**(20), 23934-23941 (2013) [doi: 10.1364/OE.21.023934].
16. Eakkachai Pengwang, Kanty Rabenorosoa, Micky Rakotondrabe, and Nicolas Andreff. "Scanning micromirror platform based on MEMS technology for medical application." *Micromachines,* **7**(2), 24 (2016) [doi: 10.3390/mi7020024].
17. Saadany, B., H. Omran, M. Medhat, F. Marty, D. Khalil, and T. Bourouina. "MEMS tunable Michelson interferometer with robust beam splitting architecture." In *IEEE/LEOS International Conference on Optical MEMS and Nanophotonics,* 49-50 (2009) [doi:10.1109/OMEMS.2009.5338601].

18. Yu Kyoungsik, Daesung Lee, Uma Krishnamoorthy, Namkyoo Park, and Olav Solgaard. "Micromachined Fourier transform spectrometer on silicon optical bench platform." *Sensors and Actuators A: Physical,* **130**, 523-530 (2006) [doi:10.1016/j.sna.2005.12.022].
19. Jack W. Judy, and Richard S. Muller. "Magnetically actuated, addressable microstructures." *Journal of Microelectromechanical systems,* **6** (3), 249-256 (1997). [doi: 10.1109/84.623114].
20. Takeshi Kobayashi, Jiunnjye Tsaur, and Ryutaro Maeda. "Fabrication of optical micro scanner driven by PZT actuators." *Japanese journal of applied physics,* **44**(9B), 7078-7082 (2005) [doi: 10.1143/JJAP.44.7078].
21. Haijun Li, Xiyu Duan, Gaoming Li, Kenn R. Oldham, and Thomas D. Wang. "An Electrostatic MEMS Translational Scanner with Large Out-of-Plane Stroke for Remote Axial-Scanning in Multi-Photon Microscopy." *Micromachines,* **8**(5), 159 (2017) [doi: 10.3390/mi8050159].
22. David Torres, Tongyu Wang, Jun Zhang, Sarah Dooley, Xiaobo Tan, and Nelson Sepúlveda. "Experimental Characterization of the Dynamics of VO2-Based MEMS Mirrors." In *ASME 2016 Conference on Smart Materials, Adaptive Structures and Intelligent Systems*, American Society of Mechanical Engineers, V001T02A005 (2016) [doi: 10.1115/SMASIS2016-9129].
23. Wataru Makishi, Yusuke Kawai, and Masayoshi Esashi. "Magnetic torque driving 2D micro scanner with a non-resonant large scan angle." In *Solid-State Sensors, Actuators and Microsystems Conference, TRANSDUCERS, International,* IEEE, 904-907 (2009) [doi: 10.1109/SENSOR.2009.5285920].
24. Arda D. Yalcinkaya, Hakan Urey, Dean Brown, Tom Montague, and Randy Sprague. "Two-axis electromagnetic microscanner for high resolution displays." *Journal of Microelectromechanical Systems*,**15**(4), 786-794 (2006) [doi: 10.1109/JMEMS.2006.879380].
25. Wei-Lun Sung, Tsung-Lin Tang, Feng-Yu Lee, Ching-Chen Tu, Ching-Han Huang, Rongshun Chen, and Weileun Fang. "Lorentz force torsional actuator with embedded nickel structures." In *Sensors, IEEE*, 1-4 (2012) [doi: 10.1109/ICSENS.2012.6411343].
26. Hee-Moon Jeong, Yong-Hwa Park, Yong-Chul Cho, Jun-Sik Hwang, Seok-Mo Chang, Seok-Jin Kang, Hyun-Ku Jeong, Jun-O Kim, Jin-Ho Lee, "Slow scanning electromagnetic scanner for laser display,"

Journal of Micro/Nanolithography, MEMS, and MOEMS, **7**(4), 043003 (2008) [doi: 10.1117/1.3033210].

27. Çağlar Ataman, Sébastien Lani, Wilfried Noell, and Nico De Rooij. "A dual-axis pointing mirror with moving-magnet actuation." *Journal of Micromechanics and Microengineering,* **23**(2), 025002 (2012) [doi: 10.1088/0960-1317/23/2/025002].
28. Elnaz Afsharipour, Byoungyoul Park, and Cyrus Shafai. "Large Tilt Angle Lorentz Force Actuated Micro-Mirror with 3 DOF for Optical Applications," In *Multidisciplinary Digital Publishing Institute Proceedings*, **1**(4), 351 (2017) [doi:10.3390/proceedings1040351].
29. Hakan Urey, "Torsional MEMS scanner design for high-resolution scanning display systems." *Optical Scanning*,**4773**, 27-38 (2002) [doi:10.1117/12.469198].
30. Robert A. Conant, Jocelyn T. Nee, Kam Y. Lau, and Richard S. Muller. "Dynamic deformation of scanning mirrors." *IEEE/ LEOS International Conference on Optical MEMS*, 49-50 (2000) [doi: 10.1109/OMEMS.2000.879621].
31. Pierre J. Brosens, "Dynamic mirror distortions in optical scanning." *Applied Optics,* **11**(12), 2987-2989 (1972) [doi: 10.1364/AO.11.002987].
32. Lobontiu, Nicolae. Dynamics of microelectromechanical systems. Vol. 17. Springer Science & Business Media, 2014.
33. Didier Raboud, Thierry Barras, F. Lo Conte, Laurent Fabre, L. Kilcher, F. Kechana, N. Abelé, and M. Kayal. "MEMS based color-VGA micro-projector system." *Procedia Engineering, Eurosensors XXIV,* **5**, 260-263 (2010) [doi: 10.1016/j.proeng.2010.09.097].
34. Chang-Hyeon Ji, Moongoo Choi, Sang-Cheon Kim, Ki-Chang Song, Jong-Uk Bu, and Hyo-Jin Nam. "Electromagnetic two-dimensional scanner using radial magnetic field." *Journal of microelectromechanical systems,* **16**(4), 989-996 (2007) [doi: 10.1109/JMEMS.2007.892897].